


# Microstructure, Enhanced Relaxor-Like Behavior and Electric Properties of $(\text{Ba}_{0.85}\text{Ca}_{0.15})(\text{Zr}_{0.1-x}\text{Hf}_x\text{Ti}_{0.9})\text{O}_3$ Ceramics

FENGYU GUO,<sup>1</sup> WEI CAI ,<sup>1,2,3</sup> RONGLI GAO,<sup>1,2</sup> CHUNLIN FU,<sup>1,2</sup>  
GANG CHEN,<sup>1,2</sup> XIAOLING DENG,<sup>1,2</sup> ZHENHUA WANG,<sup>1,2</sup>  
and QIANWEI ZHANG<sup>1</sup>

1.—School of Metallurgy and Materials Engineering, Chongqing University of Science and Technology, University Town, Shapingba District, Chongqing 401331, People's Republic of China. 2.—Chongqing Key Laboratory of Nano/Micro Composite Material and Device, Chongqing 401331, People's Republic of China. 3.—e-mail: caiwei\_cqu@163.com

$(\text{Ba}_{0.85}\text{Ca}_{0.15})(\text{Zr}_{0.1-x}\text{Hf}_x\text{Ti}_{0.9})\text{O}_3$  (BCZHT) ceramics were fabricated by a conventional solid-state reaction method. The effects of  $\text{Hf}^{4+}$  on microstructure and electric properties of BCZHT ceramics have been systematically investigated. The x-ray diffraction (XRD) results indicate that the introduction of  $\text{Hf}^{4+}$  in BCZHT ceramics induces phase transition from an orthorhombic phase to the coexistence of tetragonal and orthorhombic phases, and the lattice constant decreases with the increasing of  $\text{Hf}^{4+}$  content caused by substitution of  $\text{Hf}^{4+}$  for  $\text{Zr}^{4+}$  at B sites. As  $\text{Hf}^{4+}$  content increases, the densification of BCZHT ceramics is enhanced and the grain size increases. The introduction of  $\text{Hf}^{4+}$  at B sites results in the fall of the Curie temperature and the increase of dielectric constant in BCZHT ceramics. The temperature dependences of dielectric properties of BCZHT ( $x = 0, 0.05$  and  $0.1$ ) ceramics show obvious diffuse phase transition characteristics, and the diffuseness of phase transition is enhanced with increasing of  $\text{Hf}^{4+}$  content. But there is no frequency dispersion phenomenon in BCZHT ( $x = 0, 0.05$  and  $0.1$ ) ceramics. The substitution of  $\text{Hf}^{4+}$  for  $\text{Zr}^{4+}$  at B sites of BCZHT ceramics makes its remnant polarization increase, which results from the interaction of increased grain size and tolerance factor. When temperature is above its Curie temperature, the polarization–electric field curves of BCZHT ( $x = 0, 0.05$  and  $0.1$ ) ceramics still show nonlinear characteristics, which further proves that there is diffuse phase transition and relaxor-like behavior. Moreover, the piezoelectric coefficient of BCZHT ceramics increases as  $\text{Hf}^{4+}$  content increases.

**Key words:** Ferroelectric, dielectric properties, diffuse phase transition,  $(\text{Ba}_{0.85}\text{Ca}_{0.15})(\text{Zr}_{0.1-x}\text{Hf}_x\text{Ti}_{0.9})\text{O}_3$

## INTRODUCTION

Lead-free piezoelectric ceramics have attracted considerable attention because of their non-toxicity and excellent piezoelectric properties comparable with  $\text{Pb}(\text{Zr}, \text{Ti})\text{O}_3$  (PZT) ceramics.<sup>1,2</sup> To substitute for PZT, a series of lead-free piezoelectric materials such as ceramics based on  $\text{BaTiO}_3$ (BT),<sup>3</sup> (Bi,

$\text{Na})\text{TiO}_3$ (BNT)<sup>4,5</sup> and  $(\text{K}, \text{Na})\text{NbO}_3$ (KNN)<sup>6,7</sup> have been extensively studied. Until 2009, Liu and Ren found that  $\text{Ba}(\text{Zr}_{0.2}\text{Ti}_{0.8})\text{O}_3-x(\text{Ba}_{0.7}\text{Ca}_{0.3})\text{TiO}_3$  [i.e.  $(\text{Ba}, \text{Ca})(\text{Zr}, \text{Ti})\text{O}_3$ , or BCZT] ceramics have outstanding piezoelectric properties (the piezoelectric coefficient  $d_{33}$  of  $(\text{Ba}_{0.85}\text{Ca}_{0.15})(\text{Zr}_{0.1}\text{Ti}_{0.9})\text{O}_3$  ceramics at room temperature is 620 pC/N) caused by the existence of a morphotropic phase boundary (MPB), which results in a nearly vanishing polarization anisotropy and thus makes polarization rotation between (001)T and (111)R states easier.<sup>8</sup>

Despite their excellent piezoelectric properties, BCZT ceramics still have a few drawbacks such as low Curie temperature (60–100°C), strong temperature dependence of piezoelectric properties and high processing temperature (1300–1550°C).<sup>9,10</sup> In order to solve these problems and further improve the electric properties of BCZT ceramics, the optimization of synthesis and sintering conditions,<sup>11–13</sup> texture<sup>14,15</sup> and doping<sup>16–20</sup> have been adopted. Among them, doping is an effective and simple method to regulate microstructure and electric properties, and the introduction of dopants has been proven to improve electric properties and shift the Curie temperature of BCZT ceramics by affecting its domain structure and domain wall stability.<sup>2,21–23</sup> Zhou et al. found that the piezoelectric properties of  $(\text{Ba}_{0.85}\text{Ca}_{0.15})(\text{Zr}_{0.10}\text{Ti}_{0.90})\text{O}_3$  ceramics can be substantially improved by adding  $\text{LiTaO}_3$  [the piezoelectric coefficient  $d_{33}$  is the highest (433 pC/N) after adding 0.3 mol.%  $\text{LiTaO}_3$ ], and the Curie temperature rises from 93°C to 102°C.<sup>16</sup> Wang et al. obtained  $(\text{Ba}_{0.85}\text{Ca}_{0.15-x}\text{Pb}_x)(\text{Zr}_{0.1}\text{Ti}_{0.90-y}\text{Sn}_y)\text{O}_3$  with a high Curie temperature (125°C) and remarkable electric performance (piezoelectric coefficient  $d_{33}$  is up to 604 pC/N) by simultaneous introduction of  $\text{Pb}^{2+}$  on A sites and  $\text{Sn}^{4+}$  on B sites.<sup>18</sup> Substitution of  $\text{Pr}^{3+}$  for  $\text{Ti}^{4+}$  at B sites in  $\text{Ba}_{0.85}\text{Ca}_{0.15}\text{Zr}_{0.1}\text{Ti}_{0.9}\text{O}_3$  ceramics makes its piezoelectric coefficient and the maximum dielectric constant increase, and decreases its dielectric loss.<sup>19</sup> Moreover, the introduction of some sintering aids (such as  $\text{CuO}$ ,  $\text{Bi}_2\text{O}_3$ ,  $\text{CaO-B}_2\text{O}_3\text{-SiO}_2$ ) can lower the calcining/sintering temperature of BCZT ceramics and improve its microstructure and electric properties.<sup>24–26</sup> The chemical property and ionic radius of  $\text{Hf}^{4+}$  are similar to that of  $\text{Zr}^{4+}$ . In our previous studies,<sup>27</sup> we found that the substitution of  $\text{Hf}^{4+}$  for  $\text{Zr}^{4+}$  at B sites in  $\text{BaZr}_{0.2}\text{Ti}_{0.8}\text{O}_3$  ceramics can reduce dielectric loss and increase the remnant polarization to a certain extent. Therefore, the introduction of  $\text{Hf}^{4+}$  at B sites of BCZT ceramics may be an effective approach to improve its electric properties. However, there are very few reports on Hf-doped BCZT ceramics.<sup>28</sup> In this paper, we prepared  $(\text{Ba}_{0.85}\text{Ca}_{0.15})(\text{Zr}_{0.1-x}\text{Hf}_x\text{Ti}_{0.9})\text{O}_3$  (BCZHT) ceramics by a conventional solid-state reaction method and systematically investigated the influences of  $\text{Hf}^{4+}$  on its microstructure, dielectric, ferroelectric and piezoelectric properties.

## EXPERIMENTAL DETAILS

### Preparation

$(\text{Ba}_{0.85}\text{Ca}_{0.15})(\text{Zr}_{0.1-x}\text{Hf}_x\text{Ti}_{0.9})\text{O}_3$  ( $x = 0, 0.05$  and  $0.1$ ) ceramics were fabricated by a conventional solid-state reaction method. High-purity  $\text{BaCO}_3$ ,  $\text{TiO}_2$ ,  $\text{ZrO}_2$  and  $\text{HfO}_2$  powders, all  $\geq 99.5\%$  and purchased from Sinopharm Group Co. Ltd., were weighed in stoichiometric proportions and added into a ball milling jar. They were then milled for 8 h in distilled water and zirconia media. After the

slurry was dried, the mixture consisting of  $\text{BaCO}_3$ ,  $\text{TiO}_2$ ,  $\text{ZrO}_2$  and  $\text{HfO}_2$  was calcined at 1250°C for 4 h in air. The calcined powders were milled for 8 h and then dried. The powders with added 7 wt.% binders (15% polyvinyl alcohol solution) were compacted into disk-shaped pellets with a diameter of 10.0 mm and thickness of 1.0 mm under 20-MPa pressure. The green pellets were sintered at 1400°C for 2 h in air.

### Characterization

X-ray diffraction (XRD) data of ceramic samples were obtained using an x-ray diffractometer (Rigaku, Smartlab, Japan, 35 kV, 25 mA) with  $\text{Cu } K\alpha$  ( $\lambda = 0.15418$  nm) radiation in the range of  $2\theta$  (20°–80°) at a scanning rate of 3°/min. The density of ceramics was measured by Archimedes' method. The scanning electron microscope (Hitachi, S-3700 N, Japan) was applied to observe the surface morphology of ceramic samples. In order to measure the dielectric and ferroelectric properties, silver paste was painted on both sides of polished ceramic samples and fired at 500°C for 30 min as the electrodes. The temperature dependences of dielectric constant and dielectric loss were obtained by an LCR meter (Agilent, HP 4980A, USA) at 1 V/mm in a range from 30°C to 300°C with 2°C/min. The polarization–electric field ( $P$ – $E$ ) hysteresis loops were determined with a ferroelectric test system (aixACCT, TF2000E, Germany). To obtain the piezoelectric coefficient of BCZHT ceramics, the poling of the ceramic samples was performed at room temperature by applying a direct current (DC) field of 3 kV/mm for 30 min. The piezoelectric coefficient  $d_{33}$  was measured by a Berlincourt-type quasi-static  $d_{33}$  meter (Institute of Acoustics, Chinese Academy of Sciences, ZJ-4, China).

## RESULTS AND DISCUSSION

### Microstructure

Figure 1 illustrates the XRD patterns of BCZHT ceramics. First, the XRD patterns of all ceramic samples are very similar and show only a single phase without the evidence of an impurity phase, indicating that  $\text{Hf}^{4+}$  ions have diffused into the lattice to form  $(\text{Ba}_{0.85}\text{Ca}_{0.15})(\text{Zr}_{0.1-x}\text{Hf}_x\text{Ti}_{0.9})\text{O}_3$  solid solution. The diffraction patterns of BCZHT ( $x = 0, 0.05$  and  $0.1$ ) ceramics agree with JCPDS card no. 05-626 ( $\text{BaTiO}_3$ ,  $P4mm$ ). To find out the phase evolution, fine scanning is carried out in the diffraction angle range of 44°–46° and the results are shown in Fig. 1b. The diffraction peaks around 45° are separated by fitting the Gaussian-Lorentz line shape, and the positions of the reflections are fixed using the least square method. Generally speaking, the diffraction peaks of  $\text{BaTiO}_3$  ceramics at about 45° correspond to tetragonal (002)/(200)<sub>T</sub>, rhombohedral (200)<sub>R</sub> and orthorhombic (200)/(220)<sub>O</sub>, respectively.<sup>29</sup> As shown in Fig. 1b, BCZHT ( $x = 0$ )

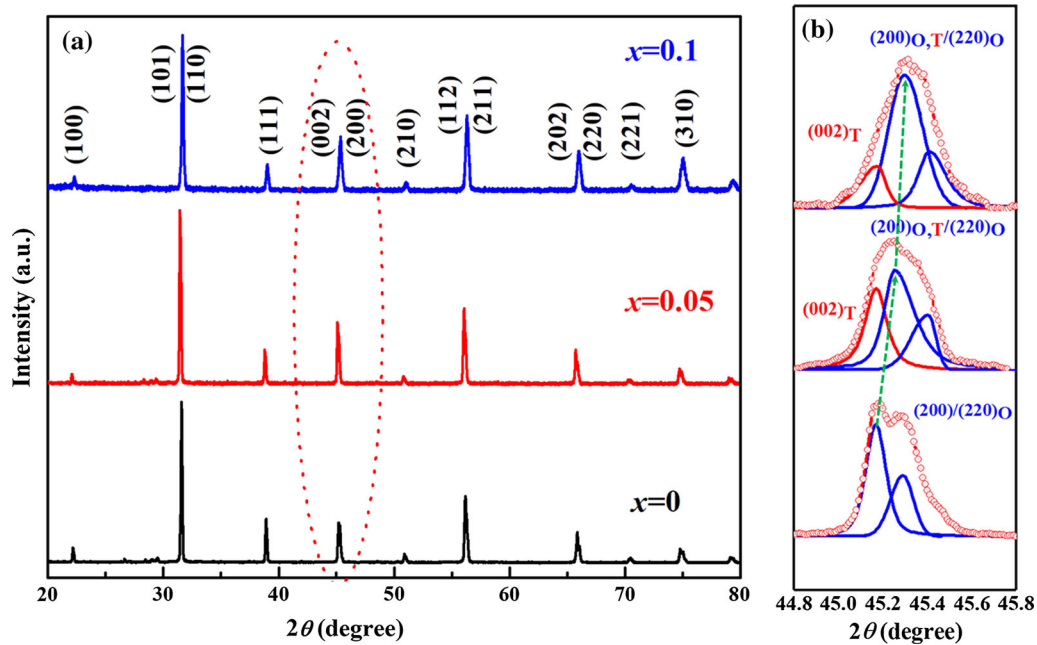


Fig. 1. XRD patterns of BCZHT ceramics.

**Table I. Lattice parameters of BCZHT ceramics**

$x$	Lattice parameters		Tetragonality
	$a$ (nm)	$c$ (nm)	$c/a$
0	4.0019	4.01135	1.0024
0.05	4.00183	4.01112	1.0023
0.1	3.99778	4.00549	1.0019

ceramics show the reflection intensity of  $(200)/(220)_O$ , which suggests the existence of an orthorhombic phase. BCZHT ( $x = 0.05$  and  $0.1$ ) ceramics show the reflection intensity of  $(002)/(200)_T$  and  $(200)/(220)_O$ , which implies the coexistence of tetragonal and orthorhombic phases. Therefore, it is concluded that the introduction of  $\text{Hf}^{4+}$  at B sites can induce the phase evolution from an orthorhombic structure to a mixture of tetragonal and orthorhombic structures. The result is in agreement with the literatures.<sup>29</sup> Second, the diffraction peaks such as  $(200)_O$  of BCZHT ceramics shift to the higher-angle region as  $\text{Hf}^{4+}$  content increases (see green arrow dash dot line in Fig. 1b), which suggests that the introduction of  $\text{Hf}^{4+}$  at B sites results in the decrease of lattice constant according to the Bragg equation ( $n\lambda = 2d\sin\theta$ ). The ionic radii of  $\text{Hf}^{4+}$ ,  $\text{Zr}^{4+}$  and  $\text{Ti}^{4+}$  are 0.079 nm, 0.080 nm and 0.068 nm respectively. Thus, the decrease of lattice constants caused by the introduction of  $\text{Hf}^{4+}$  results from the substitution of  $\text{Hf}^{4+}$  with a relatively smaller ion radius for  $\text{Zr}^{4+}$  and relatively larger

ion radius at the B sites. The lattice constant and tetragonality were calculated and listed in Table I.

To find out the influence of  $\text{Hf}^{4+}$  on grain size and densification of BCZHT ceramics, SEM was carried out to obtain the surface morphology images (shown in Fig. 2). Firstly, the average grain size of BCZHT ( $x = 0, 0.05$  and  $0.1$ ) ceramics determined by the lineal intercept method is 12.4  $\mu\text{m}$ , 14.7  $\mu\text{m}$  and 16.6  $\mu\text{m}$ , respectively, which suggests that the substitution of  $\text{Hf}^{4+}$  for  $\text{Zr}^{4+}$  at B sites increases the grain size of BCZHT ceramics. The increase of grain size can be explained by the difference in ionic radii of  $\text{Hf}^{4+}$  and  $\text{Zr}^{4+}$  at B sites. Since the ionic radius of  $\text{Hf}^{4+}$  (0.079 nm) is smaller than that of  $\text{Zr}^{4+}$  (0.080 nm), the partial substitution of  $\text{Hf}^{4+}$  for  $\text{Zr}^{4+}$  results in greater mobility of the ions, which promoted a rapid interdiffusion movement via the grain boundary, favoring the formation of necks between the grains as well as its growth and then speeding up of the grain growth.<sup>30,31</sup> Secondly, it is found that BCZHT ceramics become denser as  $\text{Hf}^{4+}$  content increases. To confirm the influence of  $\text{Hf}^{4+}$  on densification of BCZHT ceramics, the density of BCZHT ceramics was measured by Archimedes' method, and then the relative density was obtained. The relative densities of BCZHT ( $x = 0, 0.05$  and  $0.1$ ) ceramics are 94.6%, 95.7% and 97.3%, respectively, which indicates that the introduction of  $\text{Hf}^{4+}$  at B sites is helpful to obtain higher densification. The enhanced densification results from faster diffusion speed caused by  $\text{Hf}^{4+}$  with a smaller ionic radius at B sites. Moreover, it is seen that the grain of the BCZHT ceramics becomes more uniform with the increase of  $\text{Hf}^{4+}$  content.

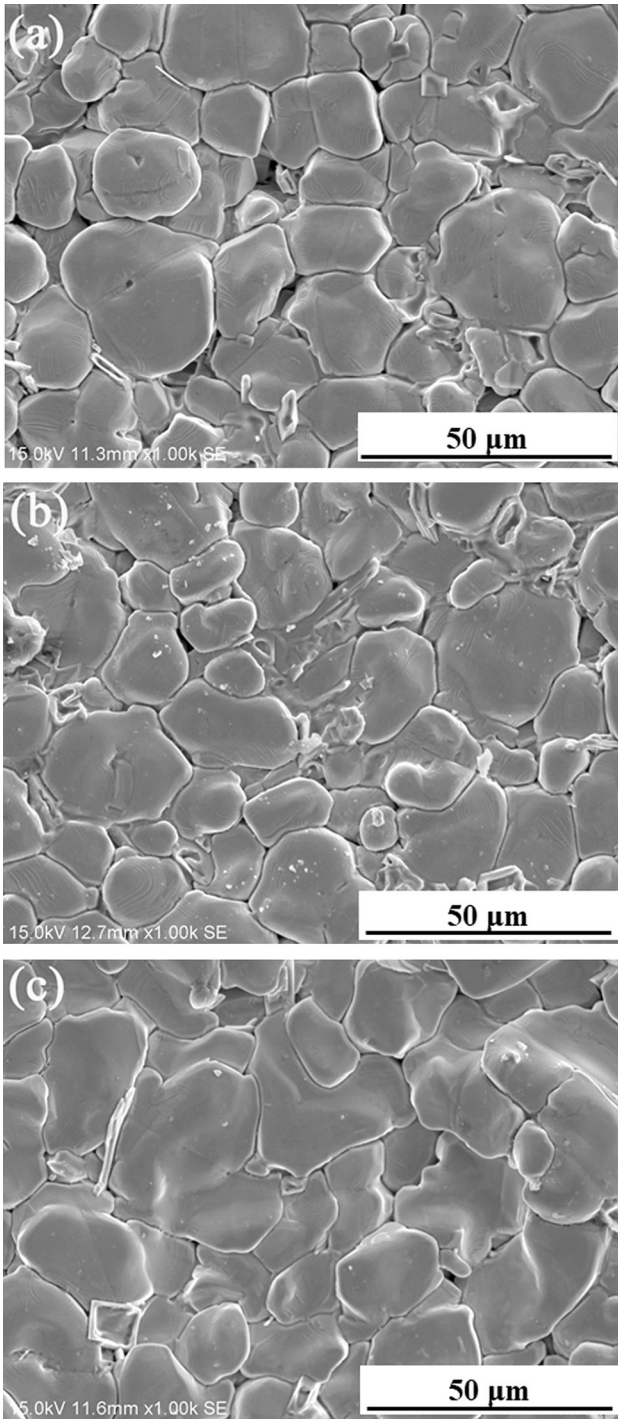


Fig. 2. SEM micrographs of BCZHT ceramics: (a)  $x = 0$ , (b)  $x = 0.05$  and (c)  $x = 0.1$ .

### Electric Properties

Figure 3 shows dielectric constant and dielectric loss as a function of temperature measured at various frequencies for BCZHT ceramics. Firstly, the dielectric constant peaks of BCZHT ( $x = 0, 0.05$  and  $0.1$ ) ceramics decrease with the increase of frequency, which is caused by different polarization mechanisms. The result reveals the dielectric

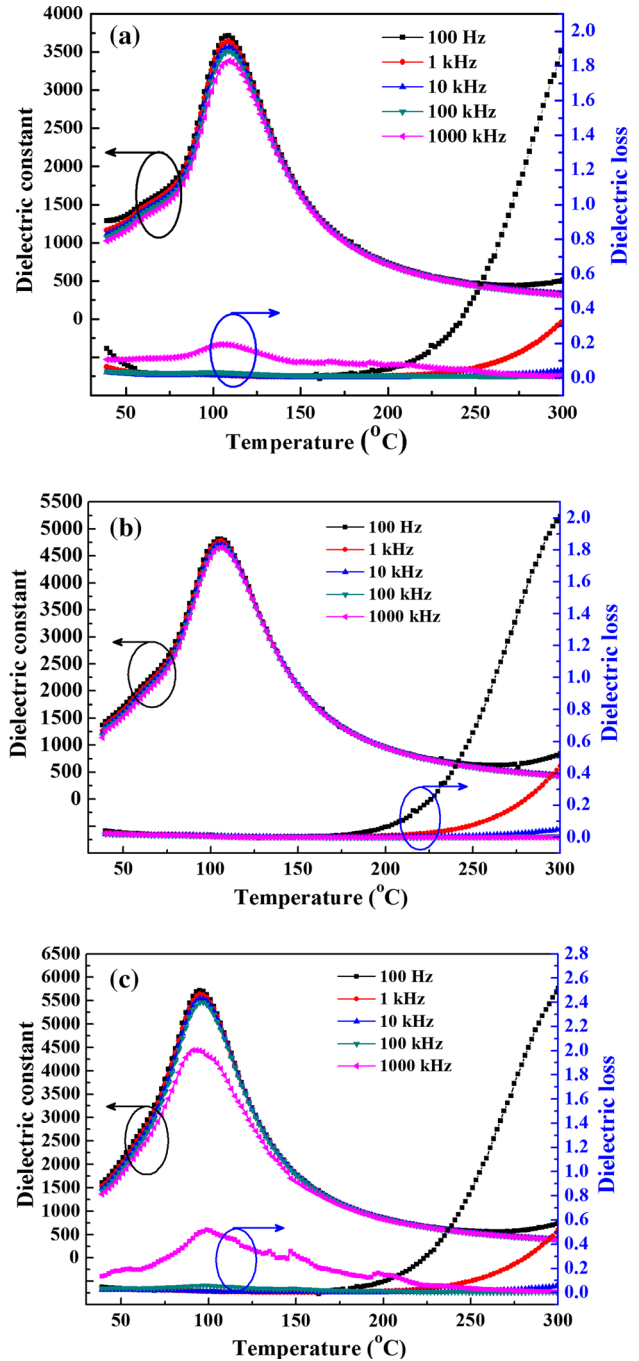


Fig. 3. Temperature dependences of dielectric constant and dielectric loss of BCZHT ceramics: (a)  $x = 0$ , (b)  $x = 0.05$  and (c)  $x = 0.1$ .

dispersion caused by a Maxwell–Wagner type of interfacial polarization.<sup>32</sup> In general, interfacial, ionic and dipole polarizations respond to a low-frequency region. As the frequency increases, the interfacial and dipole polarization gradually could not follow the change of electric field and relax down,<sup>33</sup> which leads to the decrease of the dielectric constant of BCZHT ceramics. Secondly, the Curie temperature corresponding to the maximum dielectric constant of BCZHT ( $x = 0, 0.05$  and  $0.1$ )

ceramics remains unchanged with the increase of frequency, which suggests that there is no obvious frequency dispersion in BCZHT ceramics. Thirdly, the dielectric loss of BCZHT ( $x = 0, 0.05$  and  $0.1$ ) ceramics decreases with the increase of frequency, except that there is the dielectric loss peak around  $100^\circ\text{C}$  for BCZHT ( $x = 0$  and  $0.1$ ) ceramics measured at  $1000\text{ kHz}$ . Moreover, the dielectric loss of BCZHT ( $x = 0, 0.05$  and  $0.1$ ) ceramics sharply increases with the rise of temperature when temperature is above  $200^\circ\text{C}$ , which results from increased leakage current caused by enhanced mobility of a carrier, such as electrons and holes at higher temperature.

The temperature dependences of dielectric constant and loss of BCZHT ceramics measured at  $1\text{ kHz}$  are given in Fig. 4. Firstly, it is seen that the Curie temperature ( $T_m$ ) corresponding to the dielectric constant peak of BCZHT ( $x = 0, 0.05$  and  $0.1$ ) ceramics is  $109^\circ\text{C}$ ,  $106^\circ\text{C}$  and  $95^\circ\text{C}$ , respectively, which suggests that the Curie temperature falls with the increase of  $\text{Hf}^{4+}$  content. The results are related to the change of tetragonality of BCZHT ceramics. In general, the decrease of tetragonality in  $\text{BaTiO}_3$ -based materials can make the Curie temperature fall, which is caused by the decrease of internal stress.<sup>34</sup> As mentioned above, the substitution of  $\text{Hf}^{4+}$  for  $\text{Zr}^{4+}$  at B sites of BCZHT ceramics make its tetragonality decrease, so that the Curie temperature falls as  $\text{Hf}^{4+}$  content increases. Secondly, when  $x$  increases from  $0$  to  $0.05$  and  $0.1$ , the maximum dielectric constant of BCZHT ceramics increases from  $3637$  to  $4790$  and  $5637$ . It suggests that the introduction of  $\text{Hf}^{4+}$  at B sites can increase the dielectric constant, which is mainly caused by the effect of grain size. The dielectric constant of the grain boundary in ferroelectric materials is lower than that of grain, so that the dielectric constant of the ceramic sample with larger grain size is higher than that of the sample with smaller grain size. As mentioned above, the grain size of BCZHT ceramics increases with the increasing of  $\text{Hf}^{4+}$  content, so the

maximum dielectric constant increases. Thirdly, as  $\text{Hf}^{4+}$  content ( $x$ ) increases, the dielectric loss of BCZHT ceramics slightly decreases when temperature is below  $200^\circ\text{C}$ , and the dielectric loss slightly increases when temperature is above  $200^\circ\text{C}$ . Moreover, there is obvious broadening of the dielectric constant peak corresponding to ferroelectric-paraelectric phase transition for BCZHT ( $x = 0, 0.05$  and  $0.1$ ) ceramics. The result indicates that BCZHT ceramics have a diffuse phase transition characteristic, which is associated to structural disorder and compositional fluctuations in the  $(\text{Ba}_{0.85}\text{Ca}_{0.15})(\text{Zr}_{0.1-x}\text{Hf}_x\text{Ti}_{0.9})\text{O}_3$  solid solution.<sup>35</sup>

Diffuse phase transition is generally characterized by the broadening of the maximum dielectric constant peak at the ferroelectric-paraelectric phase transition temperature, a large separation between the maxima of dielectric constant and that of dielectric loss and a deviation from the Curie–Weiss law in the vicinity of the Curie temperature.<sup>36</sup> As is well-known, the dielectric constant of a normal ferroelectric follows the Curie–Weiss law above the Curie temperature, described by

$$1/\varepsilon = (T - T_0)/C \quad (1)$$

where  $T_0$  is the Curie–Weiss temperature and  $C$  is the Curie–Weiss constant. The parameter  $\Delta T_m$ , which is often used to show the degree of the deviation from the Curie–Weiss law, is defined as follows:

$$\Delta T_m = T_{\text{CW}} - T_m \quad (2)$$

where  $T_{\text{CW}}$  denotes the temperature from which the dielectric constant starts to deviate from the Curie–Weiss law, and  $T_m$  represents the corresponding temperature of the maximum dielectric constant. Moreover, the diffuseness of the phase transition can also be described by empirical parameter  $\Delta T$ , defined as follows:

$$\Delta T = T_{0.9\varepsilon_m}(1\text{ kHz}) - T_{\varepsilon_m}(1\text{ kHz}) \quad (3)$$

where  $\varepsilon_m$  is the maximum dielectric constant,  $T_{\varepsilon_m}$  is the temperature corresponding to the maximum dielectric constant and  $T_{0.9\varepsilon_m}$  is the temperature corresponding to  $90\%$  of the maximum dielectric constant in the high-temperature side measured at  $1\text{ kHz}$ . The changes of inverse dielectric constant of BCZHT ceramics measured at  $1\text{ kHz}$  versus temperature are shown in Fig. 5.  $T_0$ ,  $C$  and  $T_{\text{CW}}$  are obtained from linear extrapolation of the inverse dielectric constant in the high-temperature region ( $T > T_C$ ) by Eq. 1, and  $\Delta T_m$  and  $\Delta T$  are obtained by Eqs. 2 and 3 (all parameters are listed in Table II). It is seen that the dielectric behavior does not completely follow the Curie–Weiss law above the Curie temperature (shown in Fig. 5).  $\Delta T_m$  and  $\Delta T$  of BCZHT ( $x = 0, 0.05$  and  $0.1$ ) ceramics are  $108^\circ\text{C}$  and  $10.1^\circ\text{C}$ ,  $116^\circ\text{C}$  and  $10.4^\circ\text{C}$ , and  $132^\circ\text{C}$  and  $12^\circ\text{C}$  respectively, indicating that the diffuseness of the ferroelectric-paraelectric phase transition of

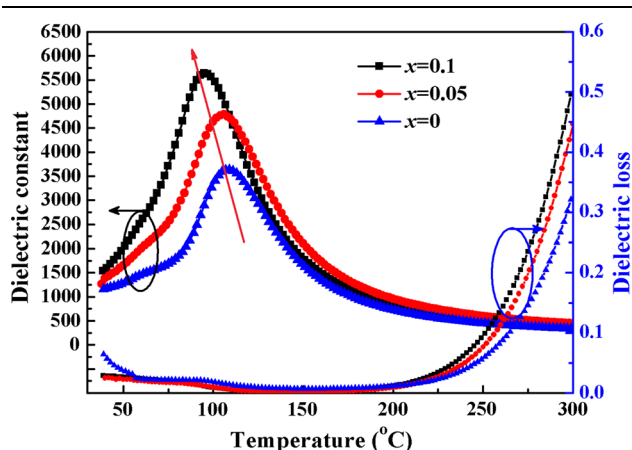


Fig. 4. Temperature dependences of dielectric constant and dielectric loss of BCZHT ( $x = 0, 0.05$  and  $0.1$ ) ceramics measured at  $1\text{ kHz}$ .

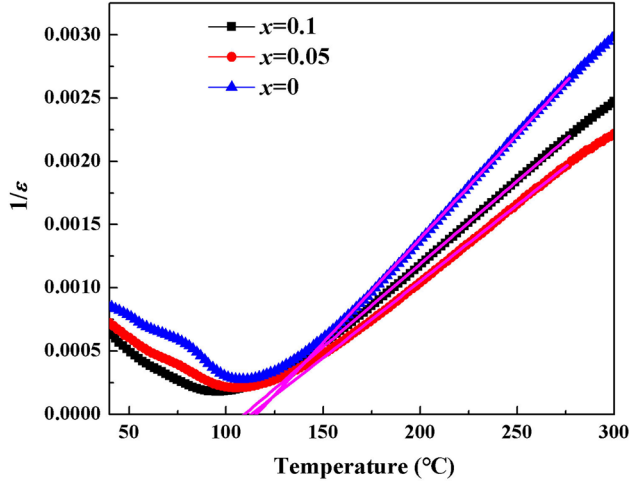


Fig. 5. Temperature dependences of the inverse dielectric constant for BCZHT ceramics measured at 1 kHz.

**Table II. The Curie–Weiss temperature ( $T_0$ ), the Curie–Weiss constant ( $C$ ),  $\Delta T$ ,  $T_{CW}$  and  $\Delta T_m$  for the BCZHT ceramics measured at 1 kHz**

$x$	0	0.05	0.1
$T_0$ (°C)	115.52	113.295	109.659
$T_m$ (°C)	109	106.0	95
$T_{0.9\epsilon_m}$ (°C)	119.1	116.4	107
$C$ ( $\times 10^5$ K)	3.3062	4.4835	6.0889
$\Delta T$ (°C)	10.1	10.4	12
$T_{CW}$ (°C)	217	222	227
$\Delta T_m$ (°C)	108	116	132

BCZHT ceramics is enhanced as hafnium content increases.

To further confirm the diffuseness of ferroelectric phase transition, a modified Curie–Weiss law was proposed to describe the diffuseness as:<sup>27</sup>

$$1/\epsilon - 1/\epsilon_m = (T - T_m)^\gamma / C' \quad (4)$$

where  $\gamma$  and  $C'$  are constant, and  $\epsilon_m$  and  $T_m$  represent the maximum dielectric constant and its corresponding temperature, respectively. The diffuseness constant  $\gamma$  defines the character of the phase transition: for  $\gamma = 1$ , a normal Curie–Weiss law is followed, whereas  $\gamma = 2$  describes a complete diffuse phase transition. To obtain  $\gamma$ , the plots of  $\ln(1/\epsilon - 1/\epsilon_m)$  as a function of  $\ln(T - T_m)$  for BCZHT ceramics are drawn and shown in Fig. 6. A linear relationship is observed for BCZHT ceramics. The slope of the fitting curves by Eq. 4 is the diffuseness constant  $\gamma$ , and some parameters are listed in Table III. It is found that the diffuseness constant  $\gamma$  increases as hafnium content increases, which also suggests that the introduction of  $\text{Hf}^{4+}$  enhances the diffuseness of phase transition. The diffuse phase transition of ferroelectric materials has generally been attributed to the existence of nano-regions resulting from local compositional fluctuation over a

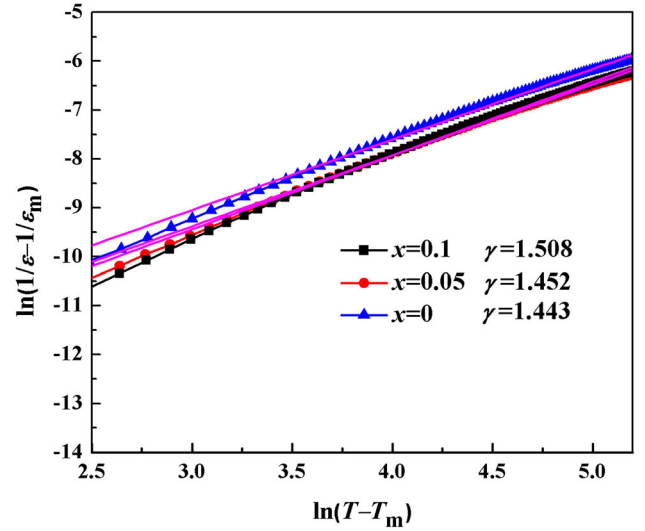


Fig. 6. Plots of  $\ln(1/\epsilon - 1/\epsilon_m)$  as a function of  $\ln(T - T_m)$  of BCZHT ceramics.

**Table III. The corresponding temperature ( $T_m$ ) of the maximum dielectric constant, the inverse maximum dielectric constant ( $1/\epsilon_m$ ) and the diffuseness constant ( $\gamma$ ) for BCZHT ceramics**

$x$	0	0.05	0.1
$T_m$ (°C)	109	106.0	95
$1/\epsilon_m$ ( $\times 10^{-4}$ )	2.74933	2.08765	1.7737
$\gamma$	1.443	1.452	1.508

length scale of 10–100 nm. The substitution of  $\text{Hf}^{4+}$  for  $\text{Zr}^{4+}$  at B sites reduces the long-order polar ordering, yielding enhanced diffuse ferroelectric phase transition. Furthermore, as mentioned above, there is no obvious frequency dispersion for BCZHT ( $x = 0, 0.05$  and  $0.1$ ) ceramics. Hence, it is concluded that BCZHT ( $x = 0, 0.05$  and  $0.1$ ) ceramics are ferroelectrics with diffuse phase transition rather than relaxor ferroelectrics.

Figure 7 shows room-temperature hysteresis loops of BCZHT ceramics measured at 100 Hz. Firstly, it is seen that the  $P$ – $E$  hysteresis loops of BCZHT ceramics show saturation characteristics. The remnant polarization ( $2P_r$ ) of BCZHT ceramics increases with the increase of  $\text{Hf}^{4+}$  content, which is caused by the interaction of grain size and tolerance factor ( $t$ ). As is well-known, the grain size of ferroelectric ceramics has a significant effect on its polarization. On the one hand, smaller grain size inhibits the formation of large ferroelectric domain and reduces the effective contribution to total polarization of ferroelectrics.<sup>37</sup> On the other hand, the grain boundary has weak ferroelectricity, which suggest that the polarization of the grain boundary may be little and even none. Space charges on the grain boundary exclude polarization charge on the grain surface so that a depletion layer on the grain surface can be formed, which results in polarization

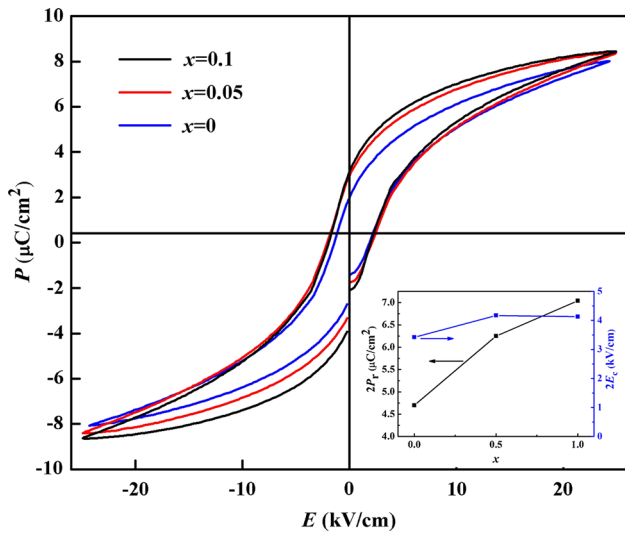


Fig. 7. Room-temperature hysteresis loops of BCZHT ceramics measured at 100 Hz (the inset is composition dependences of remnant polarization and coercive electric field).

discontinuity on the grain surface to form a depolarization field so that polarization decreases.<sup>36</sup> As mentioned above, the introduction of  $\text{Hf}^{4+}$  results in the increase of grain size of BCZHT ceramics, which leads to the decrease of remnant polarization. Moreover, it is well-known that a smaller ionic radius at B sites in  $\text{ABO}_3$  perovskite structure results in a larger tolerance factor  $t$  ( $t = \frac{r_A + r_O}{\sqrt{2}(r_O + r_B)}$ , where  $r_O$  is the oxygen ionic radius, and  $r_A$  and  $r_B$  are the ionic radii of A-site and B-site atoms). The large tolerance factor gives B-site ions enough space to move, and then leads to good ferroelectricity of  $\text{BaTiO}_3$ -based materials.<sup>38</sup>  $\text{Hf}^{4+}$  with a smaller ionic radius (0.079 nm) substitutes for  $\text{Zr}^{4+}$  with larger ionic radius (0.08 nm) at B sites, which makes the space of oxygen octahedral larger and the deviation of  $\text{Hf}^{4+}$  from the equilibrium position easier, so that the ferroelectricity of BCZHT ceramics is enhanced. Interaction of the above three aspects results in increased remnant polarization of BCZHT ceramics with the increasing of  $\text{Hf}^{4+}$  content. Secondly, the coercive electric field ( $2E_C$ ) of BCZHT ceramics initially begins to increase and then slightly decreases as  $\text{Hf}^{4+}$  content increases (shown in inset of Fig. 7). Thirdly, it is noteworthy that there is an obvious asymmetric hysteresis loop along the electric-field axis for BCZHT ( $x = 0$ ) ceramics ( $E_C^+$  is not equal to  $E_C^-$ ), as shown in Fig. 7. In other words, there is an internal electric field in BCZHT ( $x = 0$ ) ceramics, which results from the imprint process caused by defects.<sup>39</sup> It is well-known that the point defect, such as oxygen vacancy ( $V_O^\bullet$ ), forms easily during the sintering process of  $\text{BaTiO}_3$ -based ceramics. The trapped charge ( $\text{O}_2'$ ) associated with

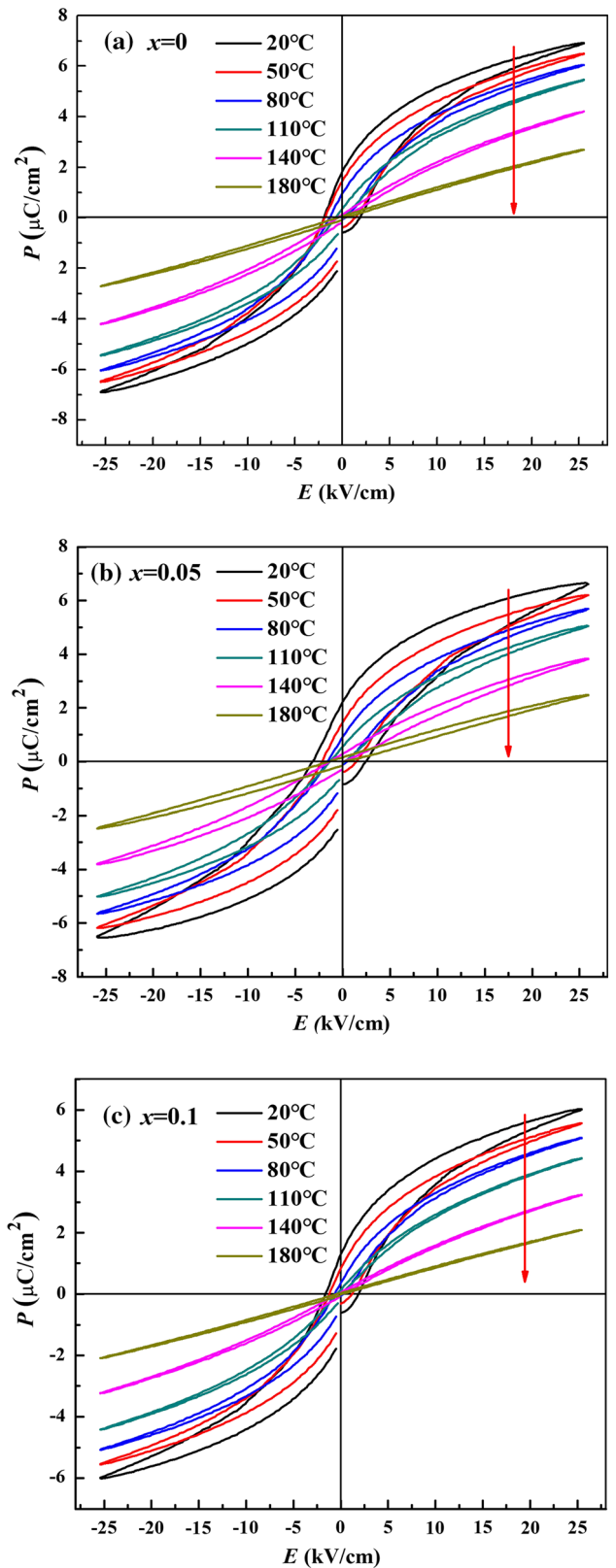


Fig. 8. Hysteresis loops of BCZHT ceramics measured at various temperature and 500 Hz: (a)  $x = 0$ , (b)  $x = 0.05$  and (c)  $x = 0.1$ .

the oxygen vacancy can promote a local stoichiometric deviation affecting the shape of the  $P$ – $E$  hysteresis loops. A significant shift of the  $P$ – $E$  hysteresis loop in BCZHT ( $x = 0$ ) ceramics is along the electric-field axis toward the positive bias as a consequence of these space charges. But the  $P$ – $E$  loop of BCZHT ceramics along the electric-field axis becomes more symmetric as  $\text{Hf}^{4+}$  content increases. The result suggests that the concentration of oxygen vacancy decreases, which is caused by the substitution of  $\text{Hf}^{4+}$  with a smaller ionic radius for  $\text{Zr}^{4+}$  with a larger ionic radius at B sites. It is because the bond strength of the  $\text{Hf}$ – $\text{O}$  bond is larger than that of the  $\text{Zr}$ – $\text{O}$  bond,<sup>40</sup> which makes the oxygen of BCZHT ceramics difficult to lose during the sintering process; this leads to the decrease of oxygen vacancy.

The hysteresis loops of BCZHT ceramics measured at various temperatures are shown in Fig. 8. Firstly, it is seen that the remnant polarization ( $P_r$ ), saturation polarization ( $P_s$ ) and the coercive electric field ( $E_c$ ) decrease simultaneously with the rise of temperature, which is due to phase transition from ferroelectric to paraelectric in BCZHT ceramics. The domain and domain wall can switch more easily at higher temperature, so that the coercive electric field decreases with the rise of temperature. Secondly, as mentioned above, the Curie temperature ( $T_m$ ) of BCZHT ( $x = 0, 0.05$  and  $0.1$ ) ceramics is about  $109^\circ\text{C}$ ,  $106^\circ\text{C}$  and  $95^\circ\text{C}$ , respectively. It is worthwhile to note that the  $P$ – $E$  curves of BCZHT ( $x = 0, 0.05$  and  $0.1$ ) ceramics still show nonlinear characteristics when temperature ( $110^\circ\text{C}$  and  $140^\circ\text{C}$ ) is above the ferroelectric–paraelectric phase transition temperature ( $T_m$ ; see the  $P$ – $E$  curves marked with dark cyan and magenta color in Fig. 8), and the  $P$ – $E$  curves measured at  $180^\circ\text{C}$  show linear characteristics. The obvious nonlinear hysteresis loops and nonzero remnant polarization in BCZHT ( $x = 0, 0.05$  and  $0.1$ ) ceramics above the Curie temperature imply that the micropolar clusters exist above  $T_m$ .<sup>41</sup> It further proves that there is diffuse phase transition and relaxor-like behavior in BCZHT ceramics. Furthermore, the piezoelectric coefficient  $d_{33}$  of BCZHT ( $x = 0, 0.05$  and  $0.1$ ) ceramics obtained by a Berlincourt-type quasi-static  $d_{33}$  meter is  $200$  pC/N,  $280$  pC/N and  $320$  pC/N, respectively. The result suggests that the piezoelectric properties of BCZHT ceramics are enhanced with the increasing of  $\text{Hf}^{4+}$  content, which is due to the increase of grain size and the phase evolution from the orthorhombic phase to the mixture of tetragonal and orthorhombic phase as  $\text{Hf}^{4+}$  content increases.

## CONCLUSIONS

$(\text{Ba}_{0.85}\text{Ca}_{0.15})(\text{Zr}_{0.1-x}\text{Hf}_x\text{Ti}_{0.9})\text{O}_3$  ( $x = 0, 0.05$  and  $0.1$ ) ceramics were prepared via a conventional solid-state reaction method.  $\text{Hf}^{4+}$  ions have diffused

into the lattice to form single-phase  $(\text{Ba}_{0.85}\text{Ca}_{0.15})(\text{Zr}_{0.1-x}\text{Hf}_x\text{Ti}_{0.9})\text{O}_3$  solid solution, and  $\text{Hf}^{4+}$  with a smaller ionic radius substitutes for  $\text{Zr}^{4+}$  with a larger ionic radius at B sites, so that the lattice constant decreases with the increasing of  $\text{Hf}^{4+}$  content. Room-temperature XRD patterns confirm the orthorhombic phase in BCZHT ( $x = 0$ ) ceramics and the coexistence of tetragonal and orthorhombic phase in BCZHT ( $x = 0.05$  and  $0.1$ ) ceramics. The introduction of  $\text{Hf}^{4+}$  enhances the densification of BCZHT ceramics and accelerates its grain growth. The introduction of  $\text{Hf}^{4+}$  at B sites results in the fall of the Curie temperature of BCZHT ceramics by decreasing its tetragonality. The maximum dielectric constant of BCZHT ceramics increases with the increasing of  $\text{Hf}^{4+}$  content. It is found that the ferroelectric–paraelectric phase transition of BCZHT ( $x = 0, 0.05$  and  $0.1$ ) ceramics have obvious diffuse phase-transition characteristics and the diffuseness of phase transition enhances as  $\text{Hf}^{4+}$  content increases. There is no obvious frequency dispersion for BCZHT ( $x = 0, 0.05$  and  $0.1$ ) ceramics. The room-temperature  $P$ – $E$  hysteresis loops of BCZHT ( $x = 0, 0.05$  and  $0.1$ ) ceramics indicate that the remnant polarization increases with the increase of  $\text{Hf}^{4+}$  content, which is caused by interaction of grain size and tolerance factor. The nonlinear  $P$ – $E$  curves of BCZHT ( $x = 0, 0.05$  and  $0.1$ ) ceramics above the Curie temperature further prove that there is diffuse phase transition and relaxor-like behavior in BCZHT ceramics. The introduction of  $\text{Hf}^{4+}$  enhances piezoelectric properties of BCZHT ceramics, which is caused by the coexistence of tetragonal and orthorhombic phase and the increased grain size.

## ACKNOWLEDGMENTS

This work was supported by the Excellent Talent Project in University of Chongqing (Grant no. 2017-35), the Science and Technology Innovation Project of Social Undertakings and People's Livelihood Guarantee of Chongqing (Grant no. cstc2017shmsA90015), the Program for Innovation Teams in University of Chongqing (Grant no. CXTDX201601032), the Leading Talents of Scientific and Technological Innovation in Chongqing, the Chongqing Research Program of Basic Research and Frontier Technology (grant nos. CSTC2018jcyjAX0416, CSTC2016jcyjA0175, CSTC2016jcyjA0349).

## REFERENCES

1. A.J. Bell and O. Deubzer, *MRS Bull.* 43, 581 (2018).
2. T. Zheng, J.G. Wu, D.Q. Xiao, and J.G. Zhu, *Prog. Mater. Sci.* 98, 552 (2018).
3. B.W. Dai, X.P. Hu, R.Q. Yin, W.F. Bai, F. Wen, J.X. Deng, L. Zheng, J. Du, P. Zheng, and H.B. Qin, *J. Mater. Sci. Mater. Electron.* 28, 7928 (2017).
4. T.Y. Li, X.J. Lou, X.Q. Ke, S.D. Cheng, S.B. Mi, X.J. Wang, J. Shi, X. Liu, G.Z. Dong, H.Q. Fan, Y.Z. Wang, and X.L. Tan, *Acta Mater.* 128, 337 (2017).
5. J. Yin, C.L. Zhao, Y.X. Zhang, and J.G. Wu, *Acta Mater.* 147, 70 (2018).



6. K. Wang, F.Z. Yao, J. Koruza, L.Q. Cheng, F.H. Schader, M.H. Zhang, J. Rödel, J.F. Li, and K.G. Webber, *J. Am. Ceram. Soc.* 100, 2116 (2017).
7. P. Li, X.Q. Chen, F.F. Wang, B. Shen, J.W. Zhai, S.J. Zhang, Z.Y. Zhou, and A.C.S. Appl, *Mater. Interfaces* 10, 28772 (2018).
8. W.F. Liu and X.B. Ren, *Phys. Rev. Lett.* 103, 257602 (2009).
9. G. Singh, V. Sathe, and V.S. Tiwari, *J. Electron. Mater.* 46, 4976 (2017).
10. Y. Nahas, A. Akbarzadeh, S. Prokhorenko, S. Prosandeev, R. Walter, I. Kornev, J. Íñiguez, and L. Bellaiche, *Nat. Commun.* 8, 15944 (2017).
11. I. Coondoo, N. Panwar, D. Alikin, I. Bdikin, S.S. Islam, A. Turygin, V.Y. Shur, and A.L. Kholkin, *Acta Mater.* 155, 331 (2018).
12. Y.S. Tian, S.Y. Li, S.L. Sun, Y.S. Gong, S.J. Sun, and Q.S. Jing, *J. Electron. Mater.* (2018). <https://doi.org/10.1007/s11664-018-6572-3>.
13. S.B. Li, C.B. Wang, X. Ji, Q. Shen, and L.M. Zhang, *J. Eur. Ceram. Soc.* 37, 2067 (2017).
14. Y.C. Liu, Y.F. Chang, F. Li, B. Yang, Y. Sun, J. Wu, S.T. Zhang, R.X. Wang, and W.W. Cao, *ACS Appl. Mater. Interfaces* 9, 29863 (2017).
15. Z.H. Zhao, X.L. Li, Y.J. Dai, H.M. Ji, and D. Su, *Mater. Lett.* 165, 131 (2016).
16. M.X. Zhou, R.H. Liang, Z.Y. Zhou, C.H. Xu, X. Nie, and X.L. Dong, *Mater. Res. Bull.* 106, 213 (2018).
17. W.F. Bai, L.J. Wang, P. Zheng, F. Wen, L.L. Li, J.W. Zhai, and Z.G. Ji, *Ceram. Int.* 44, 16040 (2018).
18. X.F. Wang, J. Liu, P.F. Liang, and Z.P. Yang, *J. Electron. Mater.* 47, 6121 (2018).
19. Ramovatar, I. Coondoo, S. Satapathy, N. Kumar, and N. Panwar, *J. Electron. Mater.* 47, 5870 (2018).
20. S. Mittal, R. Laishram, and K.C. Singh, *Mater. Res. Bull.* 105, 253 (2018).
21. T. Rojac and D. Damjanovic, *Jpn. J. Appl. Phys.* 56, 10PA01 (2017).
22. D. Damjanovic and G.A. Rossetti, *MRS Bull.* 43, 588 (2018).
23. T. Zheng, H.J. Wu, Y. Yuan, X. Lv, Q. Li, T.L. Men, C.L. Zhao, D.Q. Xiao, J.G. Wu, K. Wang, J.F. Li, Y.L. Gu, J.G. Zhu, and S.J. Pennycook, *Energy Environ. Sci.* 10, 528 (2017).
24. R. Hayati, M.A. Bahrevar, T. Ebadzadeh, V. Rojas, N. Novak, and J. Koruza, *J. Eur. Ceram. Soc.* 36, 3391 (2016).
25. Y.R. Cui, X.Y. Liu, M.H. Jiang, Y.B. Hu, Q.S. Su, and H. Wang, *J. Mater. Sci. Mater. Electron.* 23, 1342 (2012).
26. Y.M. Lai, Y.M. Zeng, X.L. Tang, H.W. Zhang, J. Han, Z.H. Huang, and H. Su, *Ceram. Int.* 42, 12694 (2016).
27. W. Cai, C.L. Fu, J.C. Gao, Z.B. Lin, and X.L. Deng, *Ceram. Int.* 38, 3367 (2012).
28. A.D. Loreto, R. Machado, A. Frattini, and M.G. Stachiotti, *J. Mater. Sci. Mater. Electron.* 28, 588 (2017).
29. X.F. Wang, P.F. Liang, L.L. Wei, X.L. Chao, and Z.P. Yang, *J. Mater. Sci. Mater. Electron.* 26, 5217 (2015).
30. J.C. Sczancoski, L.S. Cavalcante, T. Badapanda, S.K. Rout, S. Panigrahi, V.R. Mastelaro, J.A. Varela, M. Siu Li, and E. Longo, *Solid State Sci.* 12, 1160 (2010).
31. T. Badapanda, S.K. Rout, L.S. Cavalcante, J.C. Sczancoski, S. Panigrahi, T.P. Sinha, and E. Longo, *Mater. Chem. Phys.* 121, 147 (2010).
32. T. Wang, J.C. Hu, H.B. Yang, L. Jin, X.Y. Wei, C.C. Li, F. Yan, and Y. Lin, *J. Appl. Phys.* 121, 084103 (2017).
33. Y.F. Liu, Z.Y. Ling, and Z.P. Zhuo, *J. Alloys Compd.* 727, 925 (2017).
34. P. Sharma, P. Kumar, R.S. Kundu, J.K. Juneja, N. Ahlawat, and R. Punia, *Ceram. Int.* 41, 13425 (2015).
35. H. Kaddoussi, Y. Gagou, A. Lahmar, B. Allouche, J.L. Dellis, M. Courty, H. Khemakhem, and M. El Marssi, *Solid State Commun.* 201, 64 (2015).
36. X.Z. Fu, W. Cai, G. Chen, and R.L. Gao, *J. Mater. Sci. Mater. Electron.* 28, 8177 (2017).
37. J.W. Zhai, X. Yao, J. Shen, L.Y. Zhang, and H. Chen, *J. Phys. D Appl. Phys.* 7, 748 (2004).
38. N. Wang, B.P. Zhang, J. Ma, L. Zhao, and J. Pei, *Ceram. Int.* 43, 641 (2017).
39. I.B. Misirlioglu, M.B. Okatan, and S.P. Alpay, *J. Appl. Phys.* 108, 034105 (2010).
40. U. Balachandran and N.G. Eror, *Solid State Commun.* 44, 815 (1982).
41. Z. Yu, C. Ang, R.Y. Guo, and A.S. Bhalla, *J. Appl. Phys.* 92, 2655 (2002).